

Overview of Solid Particle Erosion of Helicopter Rotor Blades with Proposal

Jiaqing Li & Kanha Bhatt

University of Washington

March 23, 2025

Abstract

Helicopter rotor blade sand erosion is a notable damage mechanism for helicopters. This type of damage most commonly occurs in harsh environments where there is a heavy flow of sand particles. The most significant factors influencing solid particle erosion include impact velocity, impact angle, particle properties, and material composition. The primary damage mechanisms induced by particle erosion vary from slight surface fatigue to repeated plastic deformation. In general, a rotor blade is made up of 4 components: the leading edge, the trailing edge, the tip and the root. The blade is commonly made up of carbon or glass fiber with a metallic shielding or elastomer coating for protection against the environment. The material used must provide adequate protection while also ensuring proper aerodynamic performance of the helicopter. The goal of this work is to provide a comprehensive review of past experimental and computational studies on solid particle erosion of helicopter blades. This review will highlight key parameters and test methods that have been applied in previous research. Material properties such as hardness, elastic modulus, yield stress, and density will be discussed. Additionally, the review will explore particle-related factors, including size, impact angle, and velocity. A conclusion will be provided summarizing the results and findings from the literature review that was done. Finally, a proposal will be given outlining important factors and critical testing considerations for future work.

Background & Objective

Solid particle erosion is a major concern for helicopter rotor blades that operate in sandy environments due to its abrasive nature and potential for extensive surface damage. It is defined as material loss that occurs when surfaces are subjected to a high-velocity bombardment of particles entrained in a fluid [1]. Erosion and wear result from continuous particle flow and impingement, leading to surface degradation over time.

The most significant factors influencing solid particle erosion include impact velocity, impact angle, particle properties, and material composition. Due to the extreme operational environments helicopters often face, blade erosion has been studied. Low-altitude flights in high-wind and sandy conditions, particularly in deserts and plateaus, drastically reduce rotor blade lifespan [2]. During takeoff, hovering, or landing, the high-speed main rotors collide with airborne sand particles and experience intense collisions, leading to substantial wear. This degradation not only diminishes aerodynamic performance but also increases maintenance costs and safety risks.

Figure 1 shows a diagram defining impingement angles relative to the material surface and Figure 2 is another diagram depicting the potential damage mechanism of low-angle impact of particles.

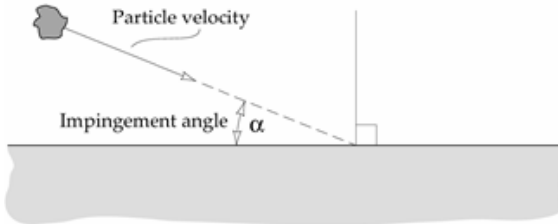


Figure 1: Impingement angle of a particle causing erosion of surface [3]

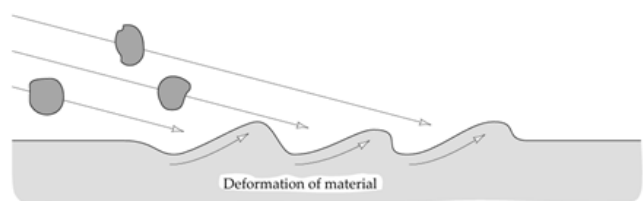


Figure 2: Lateral displacement of a material due to rippling and plowing at low impact angle [3]

The primary damage mechanisms induced by particle erosion vary from slight surface fatigue to repeated plastic deformation. As seen in Figure 3 and Figure 4, material erosion tends to exhibit brittle or ductile behavior [4]. Figure 3 shows that materials with brittle properties experience higher erosion rate and mass loss with respect to time. In contrast, materials with ductile properties initially experience solid particle accretion, followed by a gradual positive linearization of the erosion rate. Figure 4 shows that maximum weight loss of brittle materials tends to occur at high impact angles whereas ductile material mass loss peaks at lower impact angles. These images emphasize the importance of striking a balance in material properties to ensure prolonged erosion resistance across a range of impingement angles.

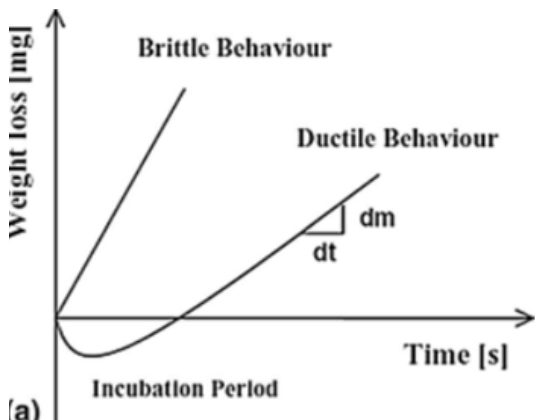


Figure 3: Erosion diagrams as a function of impact time [4]

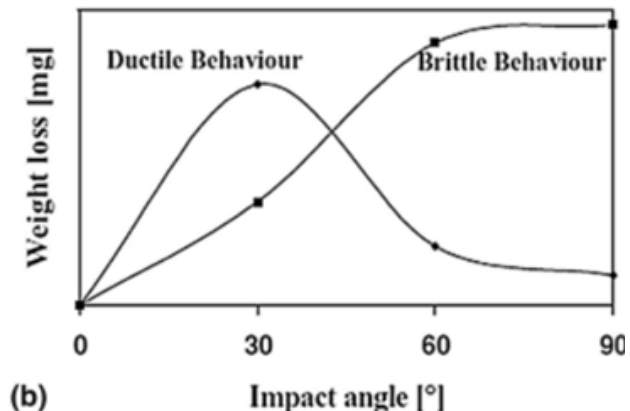


Figure 4: Erosion diagrams as a function of impact angle [4]

The solid particle damage mechanisms are illustrated in Figure 5 and Figure 6. In ductile materials, the primary erosion modes are micro-cutting, micro-plowing, and surface gouging. This type of failure is particularly evident during oblique impacts where the parallel component of the velocity vector to the surface, as shown in Figure 7, is higher [5]. In contrast, normal impacts where the force vector is normal to the target surface, as seen in Figure 8, cause significant plastic deformation. In brittle mode, the most common damage types are rapid pulverization and permanent deformation. The variation between low-angle, low-speed and high-angle, high-speed impacts influences the type of damage and failure observed on the rotor blade surface.

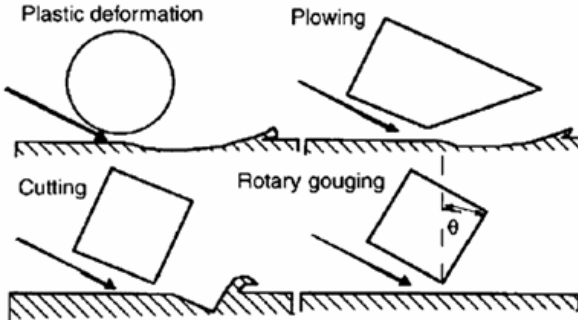


Figure 5: Mechanisms of ductile material erosion under abrasive attack [2]

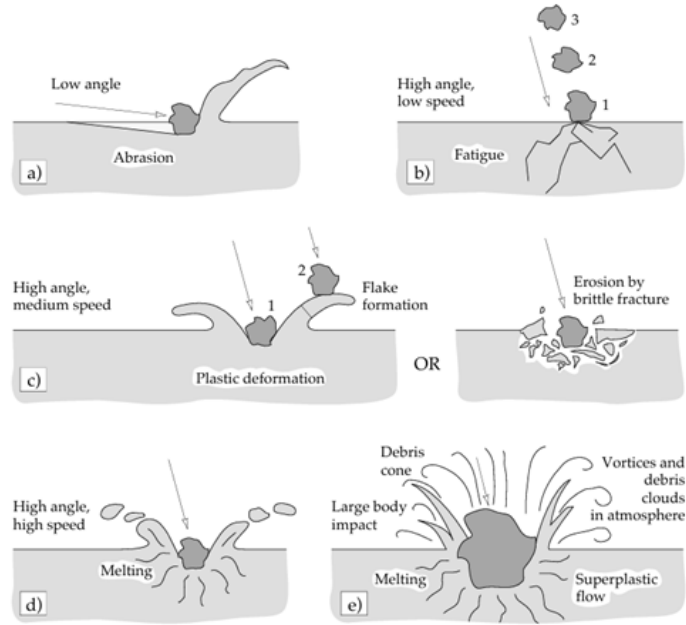


Figure 6: Possible mechanisms of erosion [3]

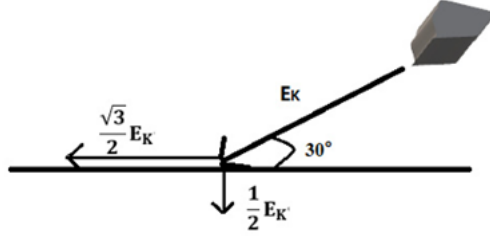


Figure 7: Erodent impact at oblique angle [5]

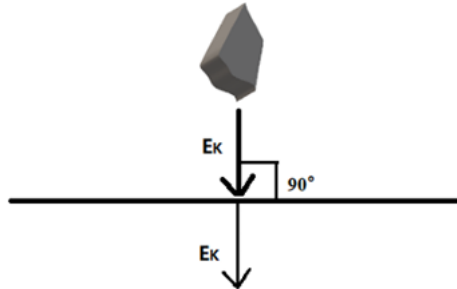


Figure 8: Erodent impact at normal angle [5]

A typical Military UH-60 helicopter is made up of four main rotor blades and four tail rotor blades. An example of this Black Hawk aircraft can be seen in Figure 9, while the structural elements of this blade can be seen in Figure 10 [6]. The lower and upper spar caps are each located on the bottom and top of the spar, respectively. These caps support the load of the entire blade, while the main and aux spar webs can bear the longitudinal shear stress.

The spar caps components are generally made-up of unidirectional carbon or glass fiber with a section of core-fittings. Some helicopter blades, made of fiber-reinforced resin matrix composites, are highly susceptible to sand erosion during low altitude flight, hovering, takeoff, and landing [5]. As a result, coatings or shielding have been developed and applied to protect composite blades from solid particle erosion [4]. The protective coating of this composite inner layer is generally accompanied by an outer layer of a metallic alloy. An example of alloys used for shielding are aluminum, titanium or steel which provide favorable aerospace-grade properties.

In general, a rotor blade is made up of 4 components: the leading edge, the trailing edge, the tip and the root. A schematic diagram of this typical design can be seen in Figure 11. The primary regions prone to damage are on the tip and on the leading edge of the blades [7]. As seen by Figure 12, the linear velocity along the blade edge increases from root to tip. The root is located at the 0.0 position of the profile length and the left and right tip are located at the -1.5 and 1.5 meter position, respectively. Assuming a constant angular velocity, the impact velocity of particles increases as the radius extends from the root to the tip.



Figure 9: UH-60 Black Hawk Helicopter
[Source](#)

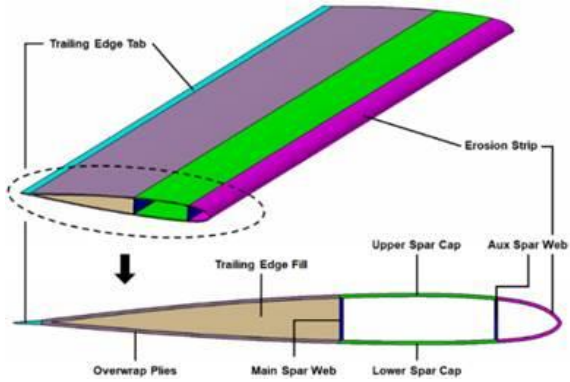


Figure 10: Structure of the main rotor blade of UH-60 helicopter [6]

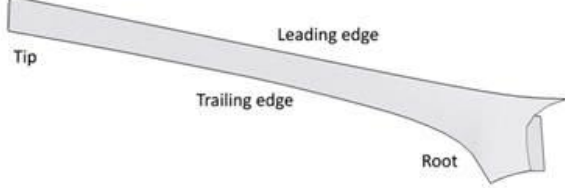


Figure 11: Components of rotor blade
[Source](#)

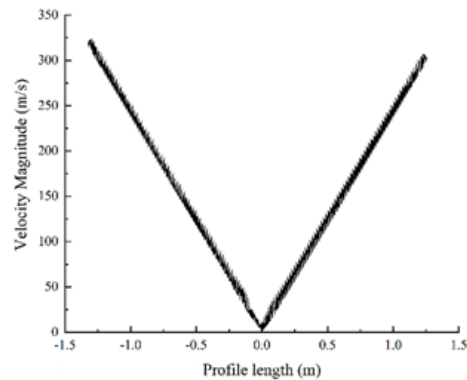


Figure 12: Linear velocity at each position of the blades [7]

Helicopters can have various tandem rotor configurations. The most common design is the single main rotor with a tail rotor, accounting for over 95% of all helicopters currently in operation [8]. Figure 13 shows five types of helicopter configurations.

In situations where the helicopter may need to carry a substantial payload, the tandem rotor is advantageous as it provides greater lift. However, a drawback of this design is the additional erosion effects caused by particle interactions [8]. Specifically, particle rebound between blades can intensify erosion damage. Figure 14 depicts trajectories of solid particles, highlighting direct and indirect collisions. The angle at which particles impact the blade influences the direction of their rebound.

Lastly, Figure 15 presents two additional operation modes that should also be considered. In helicopter mode, the rotors are positioned vertically, whereas in airplane mode, the rotors are positioned horizontally. The design and configuration of the rotor system can significantly affect blade exposure to environmental factors such as sand, dirt, and debris.

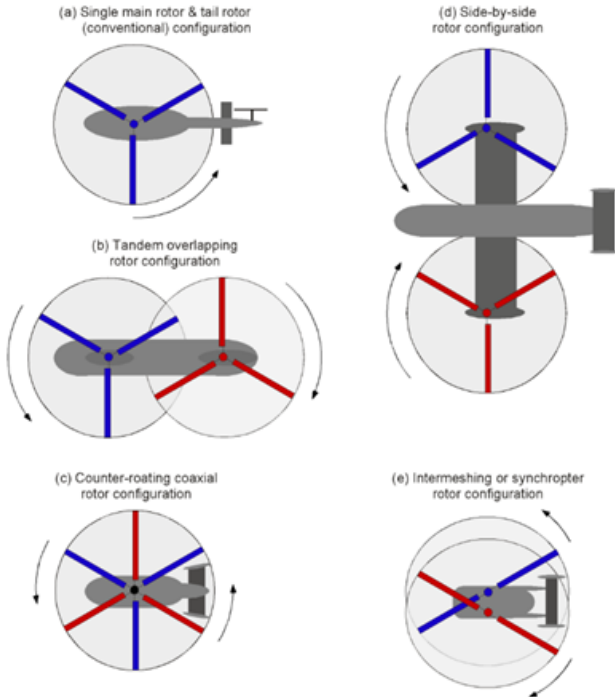


Figure 13: Components of rotor blade [8]

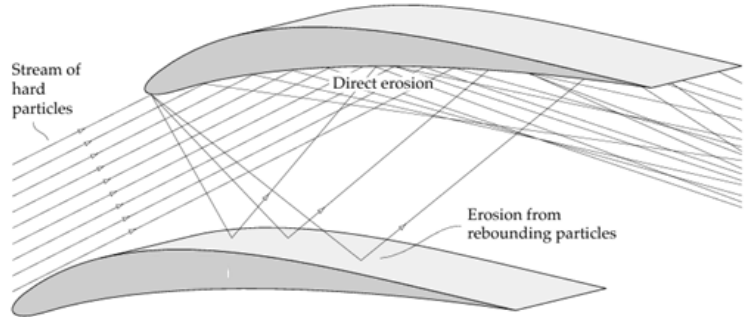


Figure 14: Particle rebound trajectory [3]



Figure 15: Aircraft Modes [8]

The purpose of this work is to provide a comprehensive review of past experimental and computational studies on solid particle erosion of helicopter blades. This review will highlight key independent and dependent variables that have been examined in previous research. Specifically, it will analyze surface properties such as hardness, elastic modulus, yield stress, and density. Additionally, it will explore particle-related factors, including size, impact angle, and velocity. Finally, a proposal will be presented, outlining key parameters and critical testing considerations.

Polymer Composite Rotor Blade Material

Helicopter rotor blades are important components that face harsh conditions in sandy environments during flight. They are primarily fabricated from fiber-reinforced resin matrix composites, commonly using carbon fiber-reinforced polymers (CFRP) and glass fiber-reinforced polymers (GFRP) [1,4]. CFRP composites typically consist of epoxy resin matrices reinforced with unidirectional or multidirectional carbon fibers, offering excellent strength-to-weight ratios and fatigue resistance [1,9]. Similarly, GFRP uses glass fibers in various configurations, as investigated by Öztürk et al. (2020), who studied E-glass fiber-reinforced silica fume and zinc oxide-filled epoxy resin composites. The orientation of fibers in both CFRP and GFRP affects the mechanical properties and erosion resistance of the blades. While these composites are lightweight and critical for aerodynamic efficiency, they are inherently vulnerable to solid particle erosion in sandy environments [9]. Sand particles can cause severe fiber fracture, delamination, and early failure of composite blades, leading to significant operational issues [5].

Erosion Effect of Different CFRP Orientations Without Coating Protection

In an early study by Kim et al. (2009), the erosion behavior of unidirectional and multidirectional CFRP composites was analyzed using twelve-layer CFRP samples. Additionally, the study examined the effects of various impingement angles (15° – 90°) and fiber orientations on erosion rates at a constant impact velocity of 70 m/s. Figure 16 illustrates particle flow impacting a CFRP surface at a specific angle, with the top layer oriented at a defined degree. Figure 17 presents the different unidirectional and multidirectional CFRP orientations used in the tests.

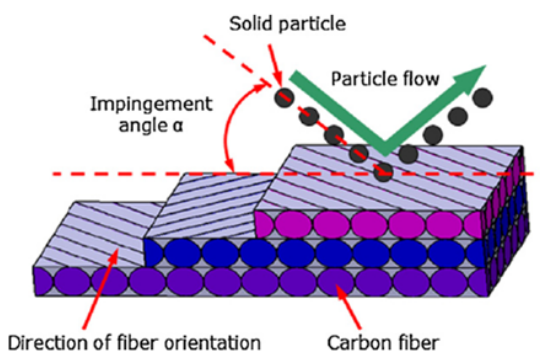


Figure 16: A diagram of erosion particle flow on sample [9]

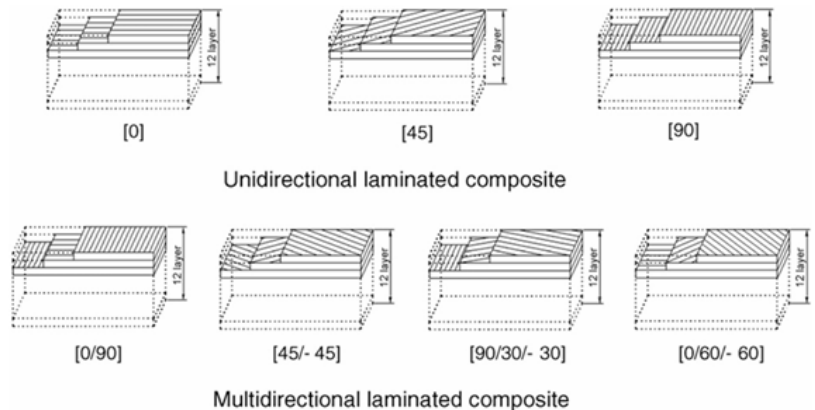


Figure 17: Fiber orientation of samples used in experiments [9]

One of the key findings of the study was the effect of impingement angle on erosion behavior. The highest erosion rate occurred at 30° , indicating ductile erosion behavior regardless of fiber orientation, as shown in Figure 18 below [9].

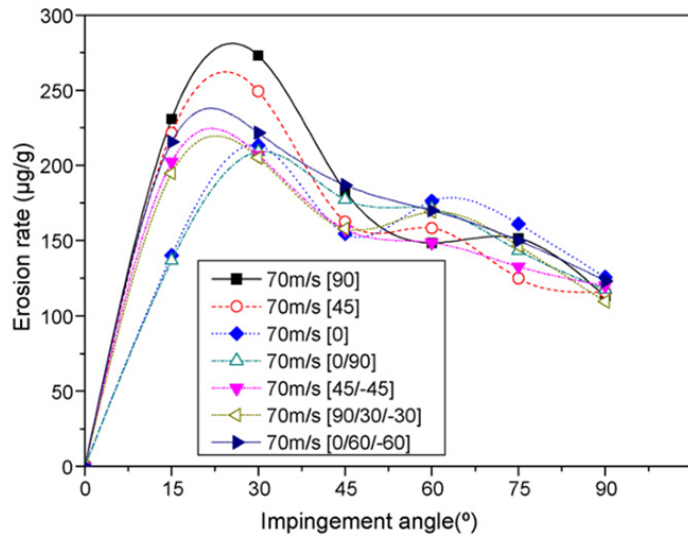


Figure 18: Variation of erosion rate at different impingement angles. The fiber volume content was 67%. The erodent was 80 µm irregular silicon carbide particles [9].

Unidirectional composites were highly sensitive to fiber orientation relative to the particle flow direction, particularly when the fiber orientation was orthogonal to the particle flow or at low angles [4,9]. In contrast, multidirectional CFRP was less sensitive due to varying fiber orientations, which provided strength in different particle flow directions.

However, two more recent studies conducted on CFRP showed brittle erosion behavior with peak erosion rate at an impingement angle of 90°, as shown in Figure 19 and Figure 22 [1,4]. In a study, by Cai et al. (2016), it was observed that at low impingement angles, the fibers remained held in place by the matrix. As the angle increased, brittle fracture of the matrix and fiber pulverization began [4]. This means it was more sensitive to impact energy.

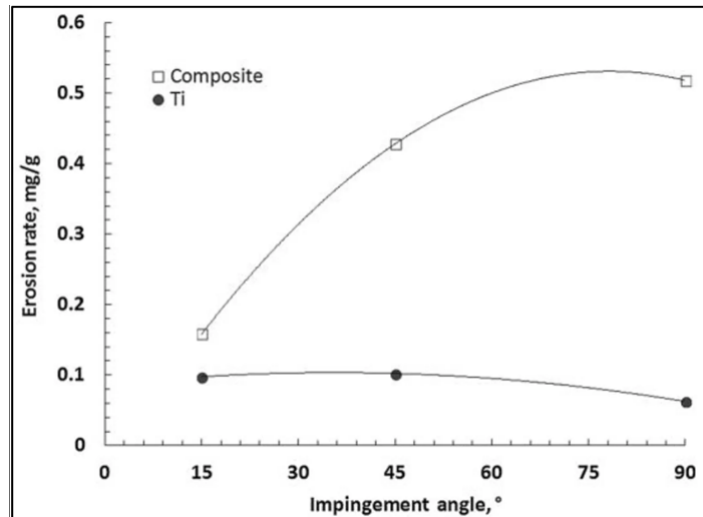


Figure 19: Erosion rate of two-layer CFRP composite as a function of impingement angle [4]

The reason for the different trend observed in the early study by Kim et al. remains unclear. However, one possible factor could be the type of resin matrix used in their CFRP. The resin matrix serves as the primary protection for the reinforcement and is the first material to be removed during surface erosion. This makes the erosion characteristics of the resin matrix crucial for the composite's overall erosion resistance, as it helps prevent fiber exposure. Another, though less likely, factor could be the difference in the number of CFRP plies (layers) used in the experiment.

Erosion Effect of GFRP with Fillers and without Coating Protection

In a separate study, Öztürk et al. (2020) investigated how filler materials such as silica fume and zinc oxide in GFRP affect the solid particle erosion rate. They specifically analyzed parameters including filler content, impingement angle, impact velocity, erosion time, and erodent particle size.

A key finding was that all GFRP samples exhibited brittle erosion behavior, with the highest erosion rate occurring at a 90° impingement angle, regardless of erodent size, as shown in Figure 20 [10]. The red arrows highlight the sample types with the highest and lowest erosion rates: FZ16 (fiber filled with 16% zinc oxide by weight) had the worst performance, while FS16 (fiber filled with 16% silica fume by weight) performed the best. This was because silica fumes absorbed some impact energy, improving erosion resistance [10]. In contrast, zinc oxide created weak interfaces, promoting crack initiation. As a result, Öztürk et al. concluded that silica fume enhances the erosion resistance of GFRP, while zinc oxide degrades it.

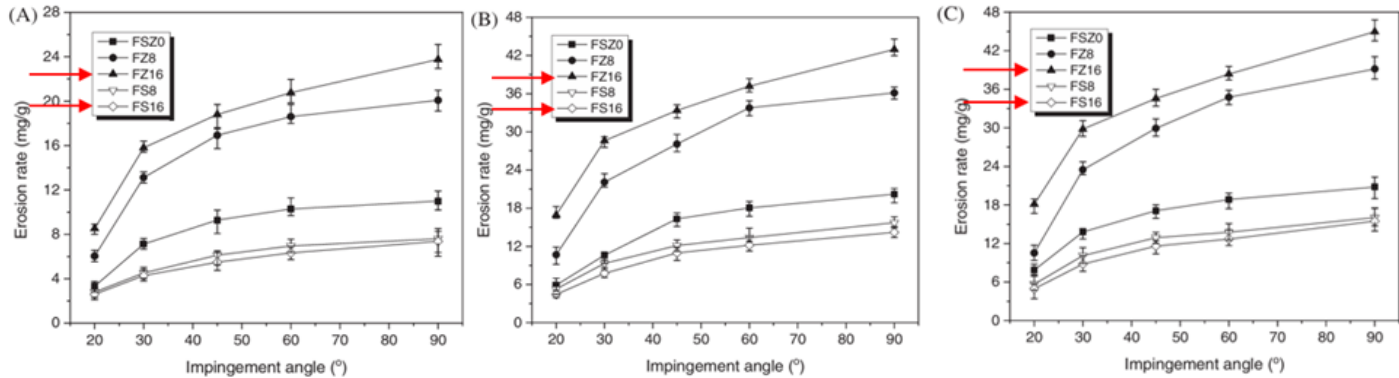


Figure 20: Effect of impact angle on erosion rate for three different erodent sizes: A: 72 μm , B: 175 μm , C: 348 μm at a constant impact velocity of 100m/s with an exposure time of 180 seconds. In the legend, F = fiber, S = silica fume, Z = zinc oxide, and the number is the filler content percentage by weight in the GFRP samples. [10]

The damage mechanism varied with impingement angle, with cutting and plowing occurring at low angles, while micro-cracking dominated at high angles [10]. One notable finding was that the erosion rate increased significantly when the erodent size increased from 72 μm to 175 μm . However, beyond 175 μm , the erosion rate stabilized, even as the erodent size increased to 348 μm , as shown in Figure 21 [10].

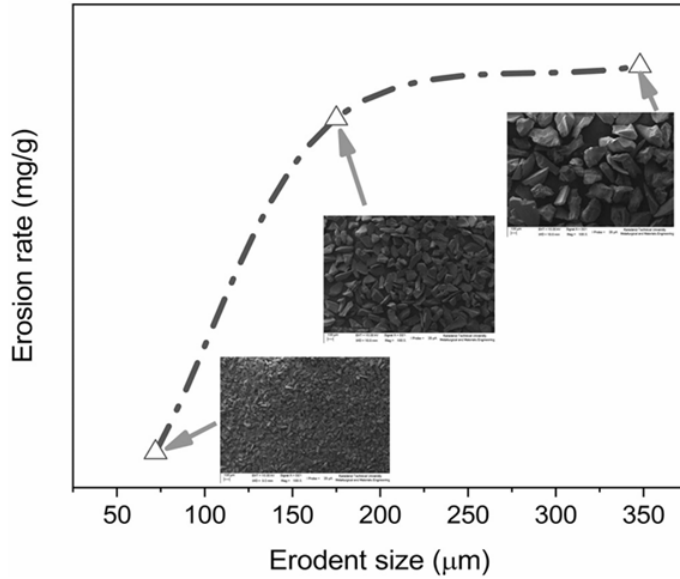


Figure 21: Variation of erosion rate due to erodent size. [10]

Öztürk et al. noted that several other studies have also concluded that the erosion rate of composites becomes independent of erodent size once it exceeds a certain critical threshold [10]. Finally, they concluded that erosion rates increase with higher impact velocity and prolonged exposure time.

Although no clear justification was provided for why erodent size has a critical value, it is an important factor to consider. In experiments where erodent particles pass through a nozzle, larger particles traveling through a fixed-diameter opening could result in a lower mass flux (fewer particles impacting a given area), leading to fewer but more forceful impacts. In contrast, smaller particles generate a higher mass flux, could result in more frequent but less intense impacts.

Experimental Studies on GFRP, CFRP, and Protective Polyurethanes

A similar study by Özen et al. (2021) analyzed erosion effects on both GFRP, CFRP, and a rotor blade protective polyurethane (PU) tape layer [1]. In their experiments, CFRP consisted of 10 layers with a 64% fiber volume ratio, while GFRP had 12 layers with a 50% fiber volume ratio. The erodent particles were 175 μm silicon carbide, with a mass flow rate of 2.5 g/min. The overall testing conditions followed ASTM-G76 standards. Özen et al. also conducted simulations to validate their experimental results.

Figure 22 illustrates how different impact angles influence erosion rates at a given impact velocity. The trends show that CFRP exhibited the highest erosion rate at 90°, indicating brittle damage behavior [1]. In contrast, GFRP had its highest erosion rate at 60°, displaying a semi-ductile-brittle behavior [1]. PU was the only material to exhibit ductile damage behavior, with the highest erosion rate occurring at 30°. Additionally, PU demonstrated the lowest erosion rate across all impact velocities and angles compared to CFRP and GFRP.

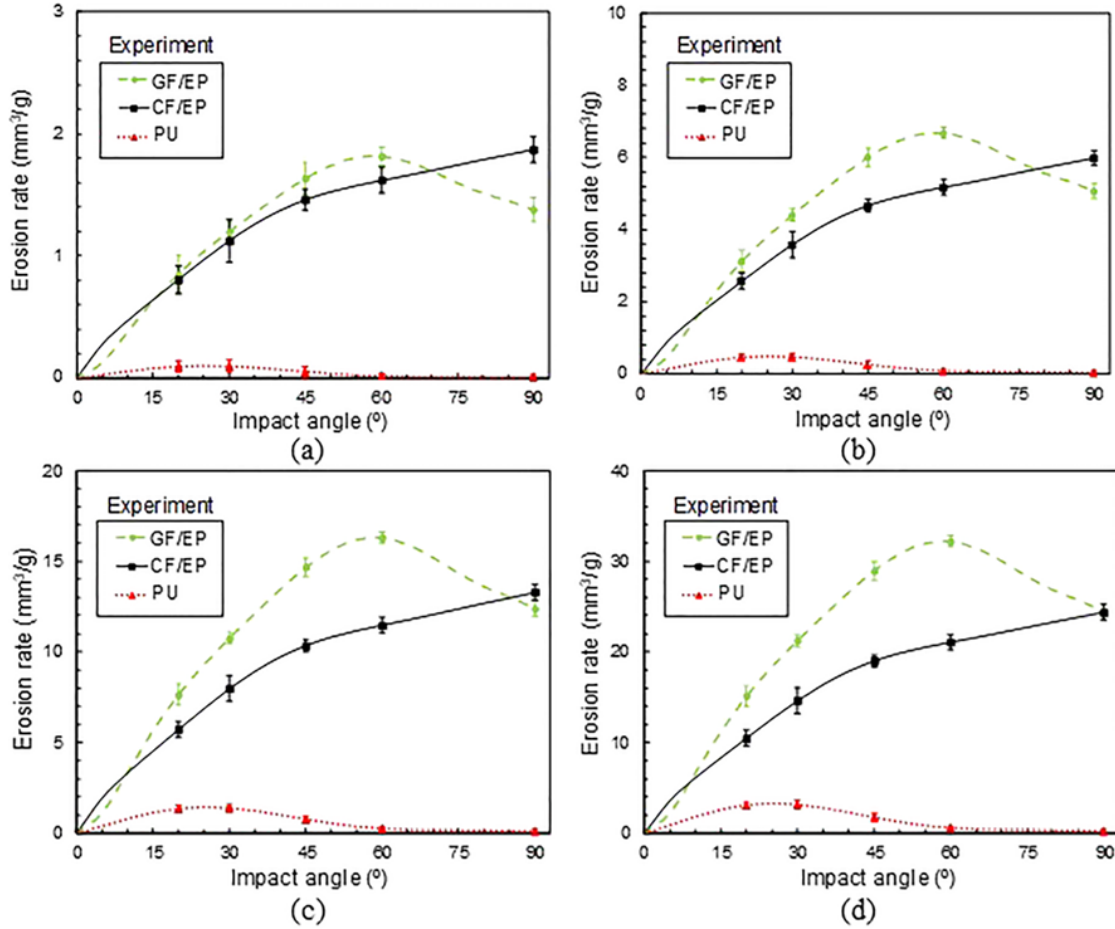


Figure 22: Experimental results and variations in erosion rates and impact angles at different impact velocities: (a) $V = 70 \text{ m/s}$, (b) $V = 110 \text{ m/s}$, (c) $V = 150 \text{ m/s}$, and (d) $V = 190 \text{ m/s}$ [1]

Computational fluid dynamics (CFD) simulations yielded similar results, as shown in Figure 23, where GFRP experienced the highest erosion, followed by CFRP, with PU tape showing the least erosion across all impact velocities [1]. The corresponding damage mechanisms are depicted in Figure 24. For CFRP at 30° , fiber cracking and fiber-matrix debonding were observed. At 90° , brittle matrix cracking, plastic deformation, and fiber pulverization occurred. GFRP exhibited similar damage mechanisms at both 30° and 90° , but the severity of the damage was significantly greater. Lastly, PU samples displayed micro-cutting and plowing at low angles, while at high angles, micro-cracking and embedded erodent particles were observed [1].

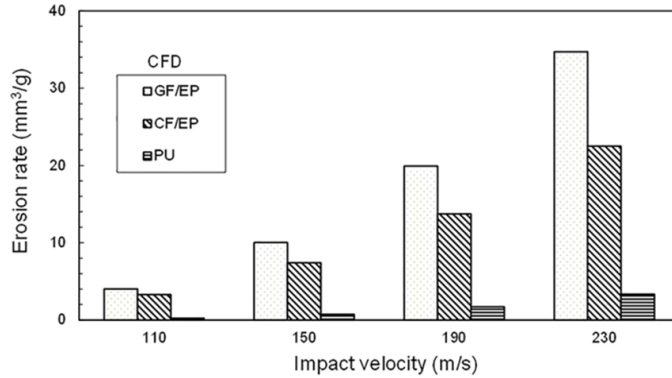


Figure 23: CFD results and comparison between erosion rates and impact velocity of GFRP, CFRP, and PU tape. [1]

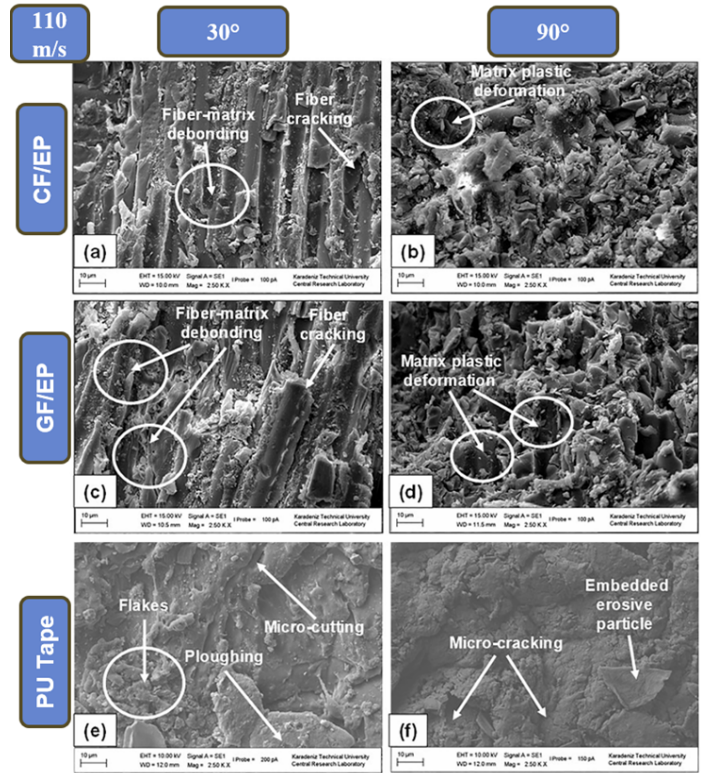


Figure 24: SEM images and damage mechanisms of the erode surfaces of CFRP, GFRP, and PU at an impact velocity of 110 m/s [1]

A study by Zheng et al. (2023) specifically examined the erosion resistance of polyurethane (PU) film on helicopter rotor blades. The PU film had a bi-layer structure, consisting of a 350 μm top layer and a 50 μm adhesive layer for bonding to a 2 mm GFRP substrate. The paper highlighted that polyurethane is an (AB) n -type linear polymer, formed by reacting a hard segment (HDMI) with a soft segment (PTMG). Furthermore, the sand erosion resistance of PU film is closely related to the hybrid ratio of these soft and hard segments, as well as the service conditions [5].

In the experiment, silica particles ranging from 80 to 120 μm were used as the erodent. The impact velocity and mass flow rate were kept constant at 220 m/s and 6 g/min, respectively, while the impact angle was varied from 30° to 90°. Additionally, the study analyzed the effects of different impact durations, ranging from 2.5 to 15 minutes.

One observation was that temperature rise increased with longer erosion time, with a maximum temperature increase of 6 °C occurring at lower impact angles, such as 30° [5]. However, due to this limited temperature increase, no significant chemical or structural changes were observed in the soft and hard blocks of the polyurethane film [5].

The general erosion trend showed that the damaged area and depth decreased as the impact angle increased [5]. Additionally, surface roughness increased more significantly at low angles due to the cutting action. At high angles, the erosion mechanism was dominated by impact action, resulting in less material loss. These two damage mechanisms contributed to different surface roughness trends, as illustrated in Figure 25. At

low impact angles, roughness increased rapidly due to cutting action, which caused wrinkling and material accumulation, leading to higher roughness [5]. After reaching peak roughness, it gradually decreased as protruding material was removed by further cutting.

In contrast, at a 90° impact angle, roughness increased more gradually and remained less severe due to the elastic rebound of sand particles [5]. The microscopic characteristics of the damage are shown in Figure 26. Plowing marks and micro-cutting were especially evident in Figure 26(b), but these damage features became less prominent as the impact angle increased. At a 90° impact angle, as shown in Figure 26(e), plowing marks were no longer present. Instead, the damage was dominated by microcracks caused by vertical impact stress [5].

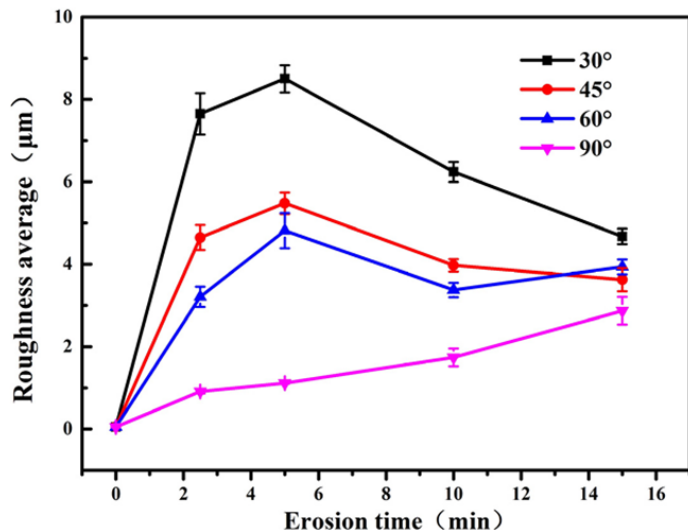


Figure 25: Changes of surface roughness with erosion time at various impact angles [5]

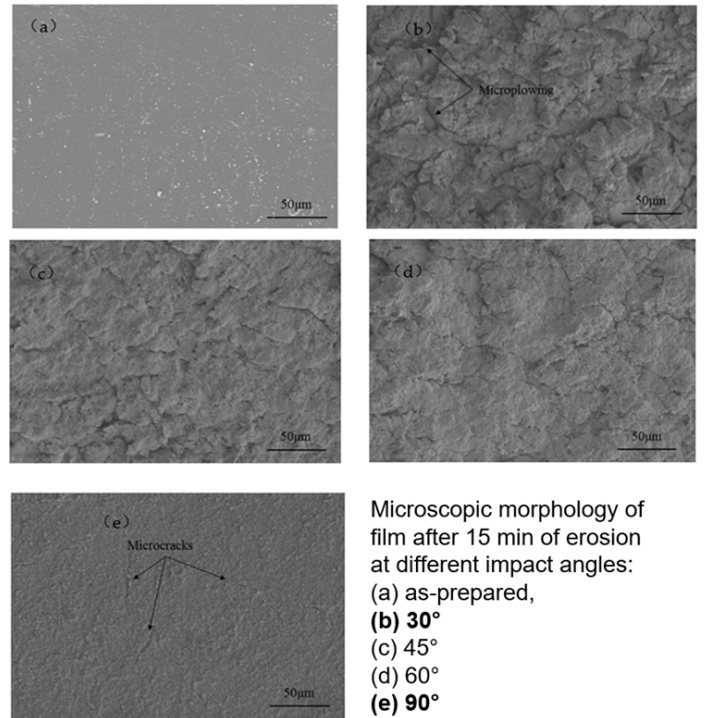


Figure 26: Morphology of film before and after 15 minute of erosion at different impact angles [5]

One important detail to note is that polyurethane is a type of elastomer where it can be stretched and deformed elastically, returning to its original shape after force is removed, as illustrated in Figure 27. Because PU films contain both soft and hardest blocks, they exhibit excellent impact absorption capacity [5]. However, with prolonged erosion exposure, small fractures can still develop at the links between these segments [5].

In fabricated PU films, the hard segments are randomly oriented and dispersed within the soft block matrix, as shown in Figure 28(a) [5]. Under stress, these disordered blocks temporarily align into a more ordered structure, as illustrated in Figure 28(b). However, due to intermolecular forces, they gradually return to their original disordered state after erosion, demonstrating a self-healing effect [5].

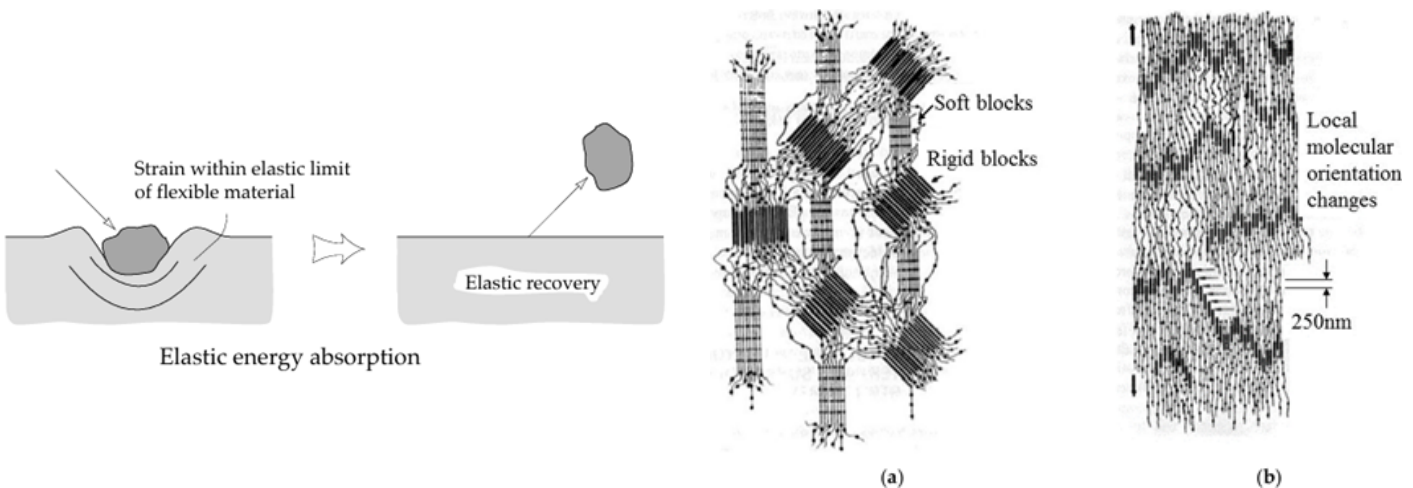


Figure 27: Illustration elastic recovery [3]

Figure 28: Changes of soft and hard blocks in PU film: (a) Disordered; (b) Locally ordered [5]

This self-healing phenomenon has also been observed in a study by Pepi et al. (2012), published by the United States military, which investigated elastomer-based protective boots, tapes, and adhesives for military helicopter rotor blades [2]. A key observation was that fine grains smaller than $75\text{ }\mu\text{m}$ could coat the elastomer surface, inhibiting the self-healing effect and thereby increasing erosion [2]. Additionally, a significant number of fine sand particles became embedded in the material, initially causing weight gain, followed by weight loss due to erosion, as shown in Figure 3. The study also confirmed that, for elastomers, the highest erosion rate occurred at an impact angle of 30° [2].

Experimental Studies on Thermoplastic Polyurethanes

A study by Arena et al. (2015) aimed to establish general relationships between erosion behavior and the key properties of thermoplastic polyurethanes (TPUs). They tested seven different TPUs from three chemical families: TPU 1 from the ether family, TPUs 2–6 from the ester family, and TPU 7 from the carbonate family. A family is defined as a group of chemically similar compounds [11].

One key finding, as shown in Figure 29, was that all TPUs exhibited their highest erosion rate at an impact angle of 15° . Among them, TPU 1 (ether-based) demonstrated the best erosion resistance, while TPU 7 (carbonate-based) had the worst [12]. All TPUs displayed ductile damage behavior, with erosion rates decreasing at higher angles.

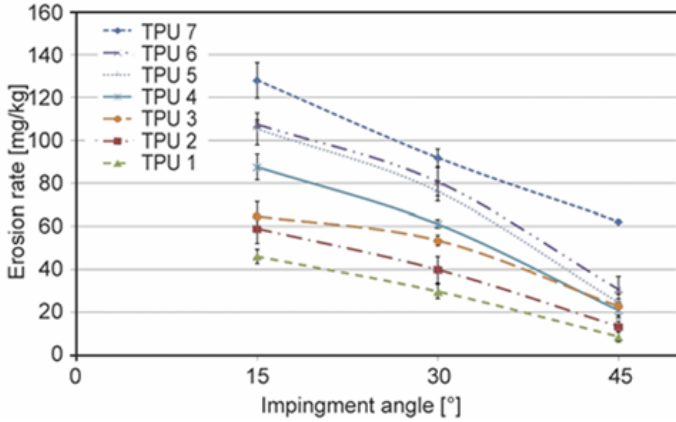


Figure 29: Variations in erosion rate of TPUs as a function of impact angles at a constant velocity of 160 m/s [12]

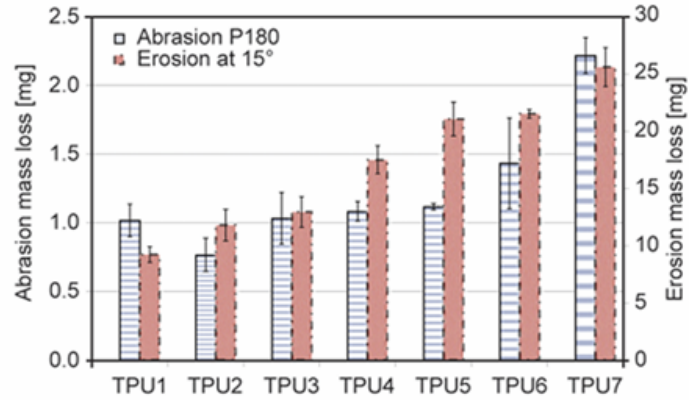


Figure 30: Comparison between mass loss by abrasion with P180 abrasive paper and the erosion data of TPUs at 15° [12]

Arena et al. also conducted abrasion tests and compared the results to the erosion rate at 15°, as shown in Figure 30. A strong correlation was found between abrasion resistance and erosion behavior at this angle, confirming similar wear mechanisms [12]. However, when attempting to correlate mechanical properties and microstructure with erosion rates, no consistent relationship was observed, as shown in Figure 31.

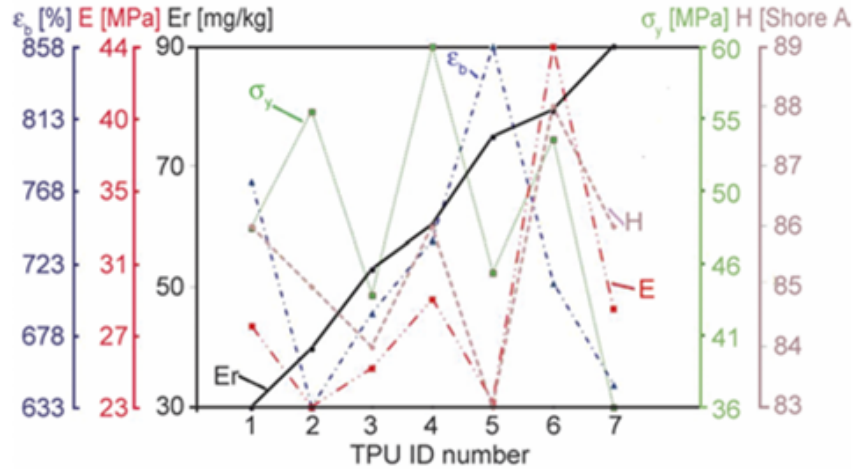


Figure 31: Comparison between erosion rate (Er) at 30° and mechanical properties such deformation at: Break (ε_b), elastic modulus (E), tensile strength (σ_y), and hardness (H) [12]

A significant correlation emerged when comparing erosion rates to viscoelastic properties, as illustrated in Figure 32 [12]. The critical frequency of 10^7 Hz was determined based on the impact duration ($\sim 10^{-7}$ s), calculated by dividing the impact depth (10 μm) by the impact velocity (160 m/s). In other words, the viscoelastic properties—specifically, the storage and loss moduli at 10^7 Hz—directly aligned with the erosion timescale [12]. While both moduli correlated with erosion behavior, the loss modulus at 10^7 Hz exhibited a stronger linear relationship with erosion mass loss compared to the storage modulus.

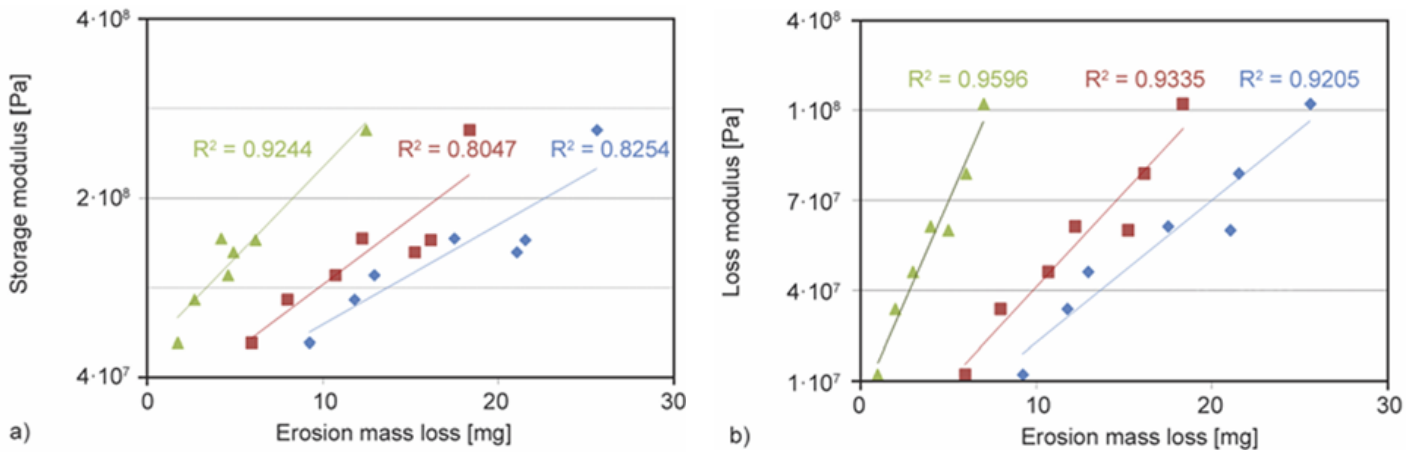


Figure 32: Storage (a) and loss (b) modulus at $w = 10^7$ Hz as a function of the mass loss at 15° (blue), 30° (red) and 45° (green) [12]

This correlation became even clearer when the moduli were normalized by mass loss, as shown in Figure 33. This method demonstrated independence from TPU type and impact angle [12]. Based on the stronger correlation with the loss modulus, all TPUs shared the same erosion resistance when evaluated through this metric [12]. In conclusion, the loss modulus at high frequencies ($\sim 10^7$ Hz) is the most reliable predictor of TPU erosion resistance [12].

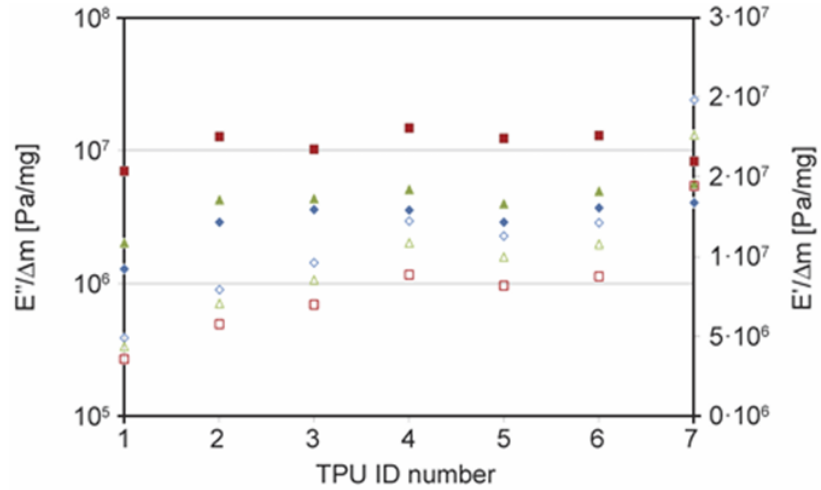


Figure 33: Storage (empty symbols) and loss (filled symbols) modulus at $w = 10^7$ Hz divided by the mass loss for all the TPUs tested at: 15° (diamonds), 30° (squares) and 45° (triangles) [12]

Computational Fluid Dynamics (CFD) Studies on Metal

Computational erosion analysis using ANSYS-Fluent has been a common method for investigating damage mechanisms on the rotor blade surface [1,7,13,14]. Through the simulation, the Discrete Phase Method (DPM) and the Euler-Lagrangian approach are applied to determine the trajectory and velocity of the particles; they are used to solve the motion equation of the particles [1,7,13,14]. The equations used and their defined variables can be seen in Figure 34 and Figure 35.

F_D (N) is the drag force per unit mass of the particle,

μ (mPa·s) is the dynamic viscosity,

U (m/s) is the fluid velocity,

V_P (m/s) is the particle velocity,

ρ_P (kg/m³) is the particle density,

g (m/s²) is the gravitational acceleration,

d_P (m) is the particle diameter,

C_D is the drag coefficient,

F_{others} (N) is other forces per unit mass,

Re is the relative Reynolds number.

$$\frac{dV_P}{dt} = F_D(U - V_P) + \frac{g(\rho_P - \rho)}{\rho_P} + F_{others}$$

$$F_D = \frac{18\mu C_D Re}{\rho_P d_P^2 \cdot 24}$$

Figure 34: Variable definitions [7]

Figure 35: Particle Motion Equation (top) and Drag Force Equation (bottom) [7]

The Beijing University of Technology Mechanical Engineering Department conducted a computational study on the effects of sand particle properties and propeller operating parameters [13]. The group simulated an aluminum alloy propeller hub and studied the effects of rotation speed, climb angle, and particle properties (the particle type was not specified). The group tested a range of climb angles from 0 to 15 degrees. It was concluded that as climb angle increases, the erosion rate is reduced; this trend can be seen in Figure 36 [13].

Furthermore, the dispersed distribution of particles is primarily concentrated at the root, the blade edge and the blade tip. Figure 37 represents a particle contour map across a range of rotational velocities from 500 – 1000 r/min. The particle mass flow rate in each figure was 0.5, 0.8, and 1.0 kg/s, respectively. A study done by Yongming Yao et al. (2021) on a Titanium Alloy shows a similar trend as seen by Figure 38. In this study, the particle mass flow rate was 0.5, 1.0, and 1.5 kg/s, respectively. The particle type was specified to be 100 um Silicon Dioxide.

These studies concluded that particle scatter is the most severe at the blade edge, especially at higher rotation speeds [7,13]. Additionally, it was determined that as particle mass flow rate increased, the erosion rates of the blades increased significantly [7,13]. The erosion rates of an Aluminum Alloy and a Titanium alloy were further examined in another study by Bai et al. (2020). This study was done alongside Yongming Yao at the Jilin University School of Mechanical and Aerospace Engineering. The goal of the study was to compare the erosion ratio of 3 different metallic alloys [14]. The erosion ratio is defined as the volume fraction of material

loss per kg of impacting particles. The results of comparison across different impact speeds can be seen in Figure 39. As seen in the bar chart, the Magnesium Alloy (Mg-Li9-A3-Zn3) performed the worst at all speeds, the Titanium Alloy (Ti-4Al-1.5Mn) performed the best, and the Aluminum Alloy (Al7075-T6) showed intermediate performance.

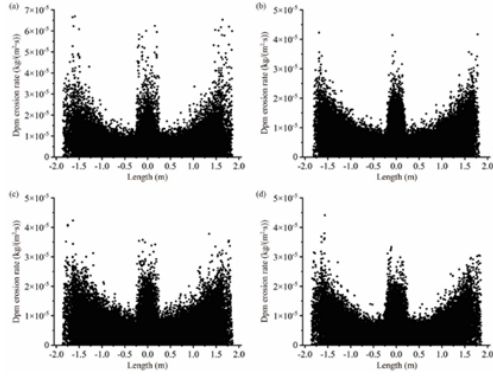


Figure 36: Erosion Rate over blade length. Climb Angles: (a) 0° , (b) 5° , (c) 10° , (d) 15° [13]

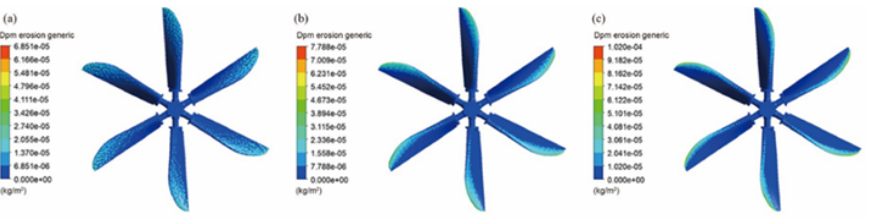


Figure 37: Erosion Rate over Rotational Velocity (a) 500 r/min , (b) 800 r/min , (c) 1000 r/min [13]

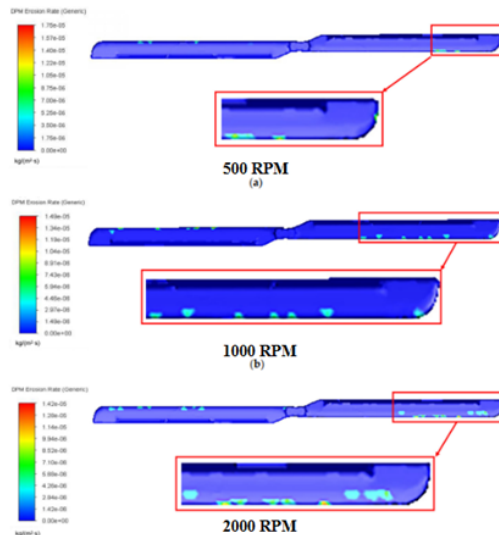


Figure 38: Erosion Rate over Rotational Velocity (a) 500 r/min , (b) 1000 r/min , (c) 2000 r/min [7]

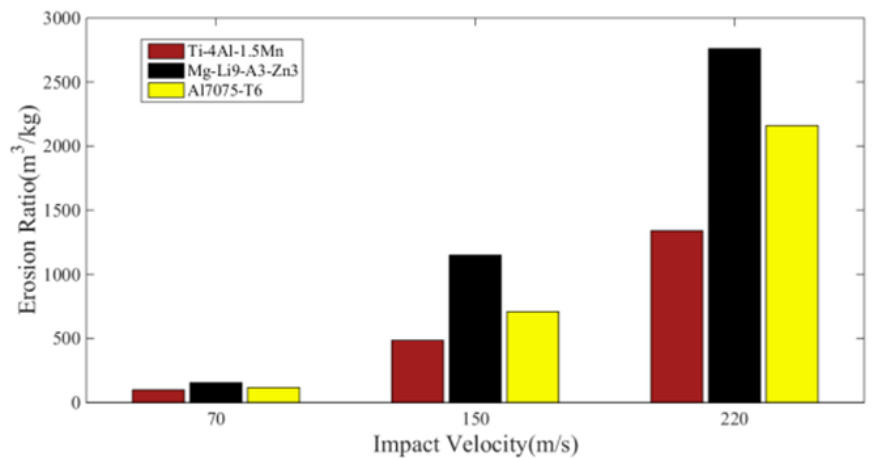


Figure 39: Erosion ratios of three materials at different impact speeds [14]

The Beijing University of Technology Mechanical Engineering Department also looked into the impact of surface roughness on the aerodynamics [13]. Specifically, Guo et al. (2025) looked into the effect on thrust generation and power consumption of the aircraft. Figure 40 depicts the relationship between the propeller thrust coefficient (C_T) and the power coefficient (C_P) with respect to roughness (K_s). It can be seen that as

roughness increases, both (C_T) and (C_P) display a declining trend when the blade edge and pressure side (underside of the blade) are uniformly roughened (black line). Additionally, at a roughness value of 500 μm , the power loss reaches 4.4% [13]. The red line on the figure displays the blade edge roughness being held constant (500 μm) while the pressure side roughness is varied. When roughness was applied only to the pressure side, a noticeable decrease in both C_T and C_P occurred. These results show that erosion-induced roughness degrades propeller performance, with pressure side roughness being the primary contributor [13].

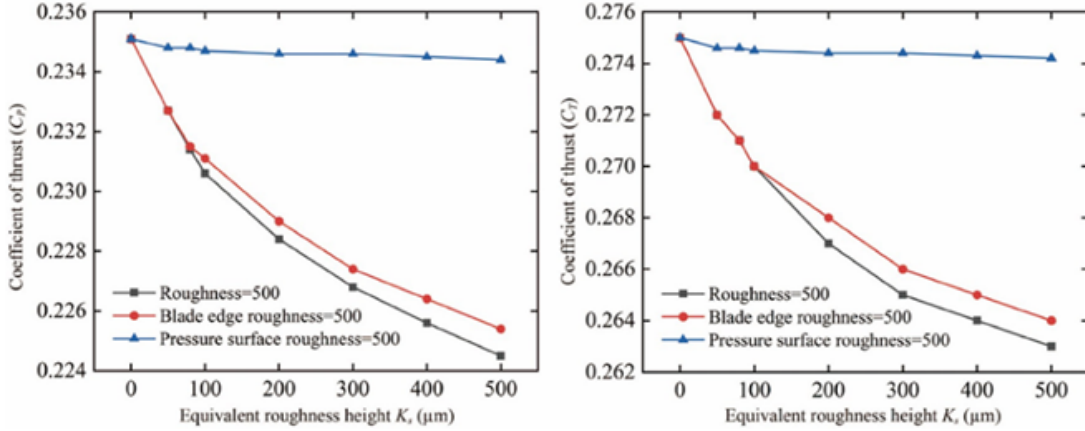


Figure 40: Thrust coefficients and Power coefficients and for different roughness cases [13]

A numerical study by the Department of Mechanical Engineering at Karadeniz Technical University (Turkey) looked into solid particle erosion performance with stainless steel (SS304) and pure nickel (Ni) [1]. These materials are commonly used as the shield surface of the helicopter rotor blades [1]. The group used ANSYS-Fluent and applied the particle flow equation. The tests were conducted at room temperature using silica (SiC) particles (average diameter of 175 μm) as an erodent. Erosion behaviors on the shield surface were investigated under different impact velocities (110, 150, 190, and 230 m/s) at a pitch angle of 0°. Figure 41 depicts the erosion rate over varying impact velocities for SS304, Nickel, PU/SS304, and Pu/Ni (hybrid shields). The bar chart shows that the use of PU tape material improves the erosion resistance at lower impact velocities (below 150 m/s). However, as the impact velocity increases (190 to 230 m/s), the PU tape becomes more erodible compared to the SS304 and the Nickel. Furthermore, the author states that PU tape can be used as protective surface material in the regions of high impact angles (from 60° and 90°) [1].

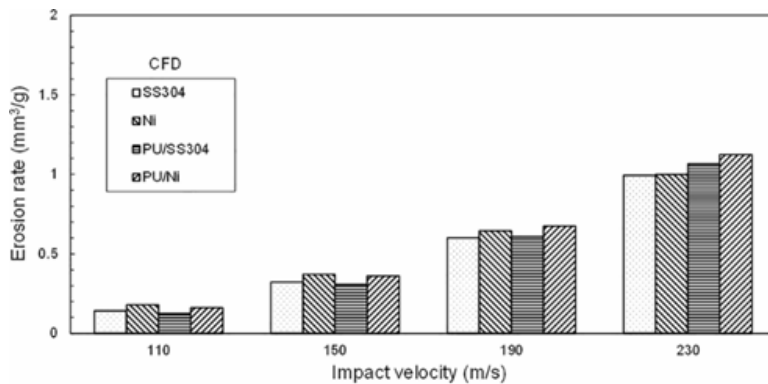


Figure 41: Erosion Rate versus Impact Velocity for different Shield surfaces [1]

Experimental Studies on Metal

Experimental erosion analysis using particle impingement testing has been a common method for investigating damage mechanisms on the rotor blade surface [1,2,15–18]. ASTM G76-05 is the Standard Test Method for conducting erosion tests by solid particle impingement using gas jets. MIL-STD-3033 is the United States Department of Defense Test Method Standard for particle and sand erosion testing of rotor blade protective materials.

In a study by Pepi et al. (2011), the Army Research Laboratory (ARL) and the University of Dayton Research Institute (UDRI) conducted erosion testing. The goal of the study was to determine the erosion resistance of materials currently used on the leading edges of Army aviation rotor blades of aircrafts in Southwest Asia (SWA) [2]. The experimental testing involved three sand sizes: Afghanistan Sand (38 – 250 μm), Gulf Sand (240 – 550 μm), and Foundry Sand (177 – 250 μm). In phase I of the study, the group tested uncoated electroformed nickel, uncoated AM355 stainless steel, and uncoated Ti-6Al-4V. Figure 42 depicts the test schematic and Figure 43 represents the actual test rig used for experimentation. The materials were tested at angles of impingement ranging from 20° to 90° , with an impact velocity from 155 to 365 m/s. The velocity was chosen to simulate different helicopter hover conditions, where the blade tips travel 212 – 242 m/s [2]. The results of the testing found that Afghanistan causes the highest metallic erosion rate between 30° to 60° . Gulf sand and Foundry sand show their highest metallic erosion rates at 30° and 60° , respectively [2]. It was also noted that a higher modulus of elasticity in metal will yield a higher erosion resistance [2]. The hardness and young modulus values for each metal are shown in Figure 44.

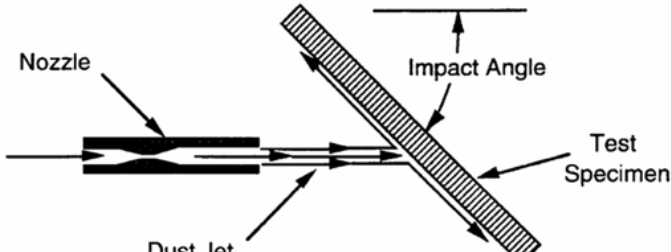


Figure 42: Particle erosion schematic [2]

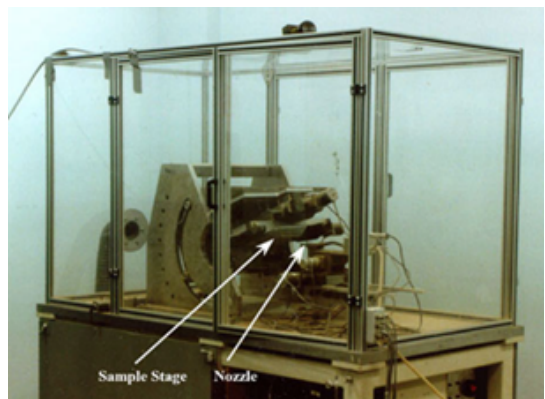


Figure 43: Dust erosion chamber at UDRI [2]

| Material | Average hardness (HRC) | Young's modulus ($\times 10^6$ psi) |
|-----------------------|------------------------|--------------------------------------|
| Electroformed nickel | 25.7 | 30.0 |
| Titanium (Ti-6Al-4V) | 32.5 | 16.5 |
| AM355 stainless steel | 33.1 | 29.4 |

Average of ten readings, Rockwell "C" Scale, 150 kgf major load

Figure 44: Metallic erosion sample hardness test results [2]

A similar study was done by Nguyen et. al (2014) to investigate erosion characteristics of stainless steel under high impact velocity. The group ran the study using Alumina particles (145 μm) at a constant velocity of 200 m/s with impact angles ranging from 10°- 90°. The test was done on a stainless steel surface (SUS304) which had a Brinell Hardness of 187 HB and a tensile strength of 616 MPa. The group concluded that the maximum erosion occurred at a 40° impact angle, which is consistent for ductile materials [17]. Due to the nature of stainless steel material having a face-centered cubic lattice structure, the slip plane (111) is inclined at 40°- 45° to the horizontal surface direction, which helps the action of removing material easier [17]. It was observed that erosion mechanisms transitioned from micro-cutting and plowing at low angles to indentation-induced plastic deformation at high angles [17]. The group further validated their results by applying CFD modeling.

A study on metallic erosion was also conducted by Yang et. al (2023). The objective was to compare the erosion resistance of Aluminum Titanium Nitride (AlTiN) and Titanium Nitride (TiN) coatings. It is stated that high hardness is required to reduce mechanical cutting by erodent particles, whereas high toughness is needed to resist brittle erosion damages [19]. The group tested the performance of these coatings on alpha-beta Titanium alloy (Ti6Al4V) flat coupons; the coating thickness was \sim 15.4 μm . The particle velocity was varied from 84 to 250 m/s while testing impingement angles from 30° to 90°. Testing was carried out using a Gas Jet Sand Erosion Tester (Alumina particles with 106 μm size) and a Dynamic Wind Tunnel Erosion Tester (Silica particles with 100 μm size). The two test setups can be seen in Figure 45 and 46. At an impact speed of 150 and 200 m/s, the AlTiN coating exhibited lower erosion rates across all angles. The performance of both coatings can be seen in Figure 47. In Figure 48, it can be seen that the AlTiN coating outperforms TiN in erosion resistance at high angles and high particle velocity [19]. The SEM images comparing the eroded surfaces of both coatings can be seen in Figure 49 and 50. The AlTiN coating shows a much smoother surface morphology. The higher erosion resistance of the AlTiN coating is attributed to a combination of higher hardness against micro cutting and higher toughness against crack formation and chipping [19].

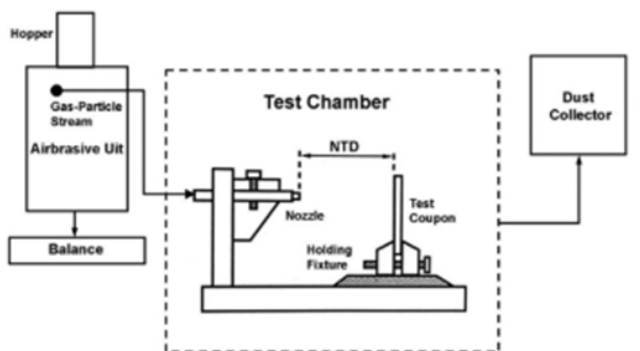


Figure 45: Schematic of gas erosion testing using Alumina particles [19]



Figure 46: (a) Test setup for the wind tunnel dynamic erosion testing, (b) the propeller blade and (c) the sharp-edged SiO₂ particles [19]

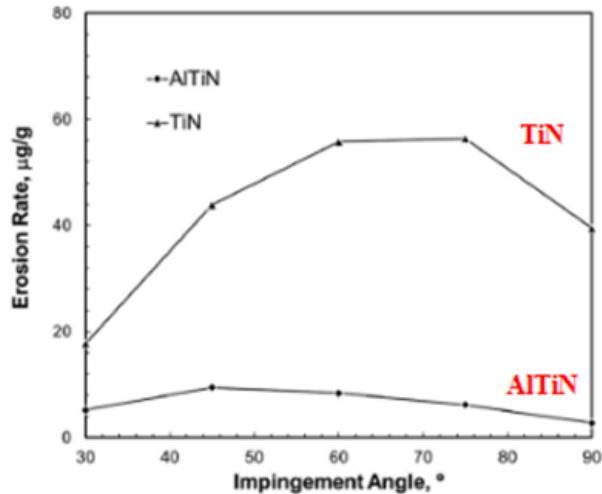


Figure 47: Gas Jet Experiment: Erosion rate of AlTiN and TiN coatings at particle velocity of 150 m/s [19]

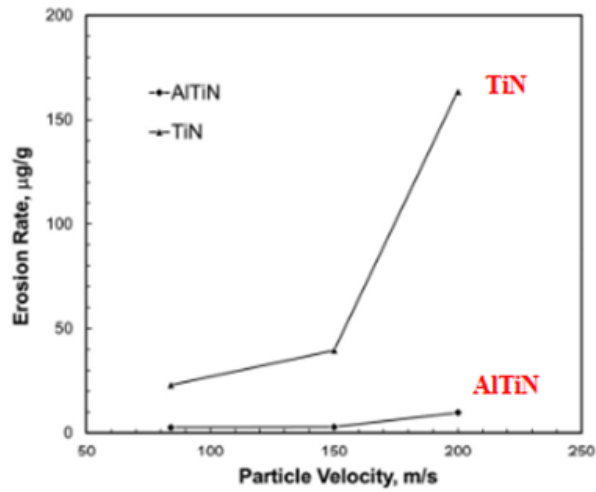


Figure 48: Gas Jet Experiment: Erosion rate of AlTiN and TiN coatings at a impact angle of 90° [19]

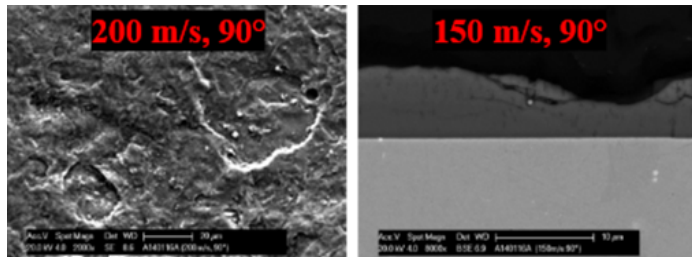


Figure 49: SEM images showing the eroded surfaces of TiN coating [19]

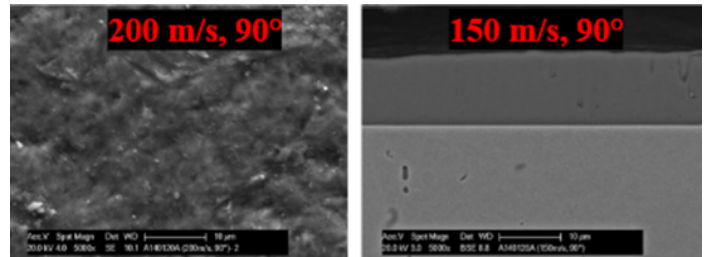


Figure 50: SEM images showing the eroded surfaces of AlTiN coating [19]

Ozen et. al (2021) also looked into rotor blade shielding using a metallic coating. The group conducted testing according to ASTM G76, ASTM F1864, and MIL-STD-3033 standards. The test used silicon carbide (SiC) particles with an average diameter of 175 um. A range of impact velocities (70 to 190 m/s) and impact angles (20° to 90°) were tested. Figure 51 and Figure 52 show that the maximum erosion rate for SS304 and Nickel occurred at 20°; this is an indicator of ductile damage [1].

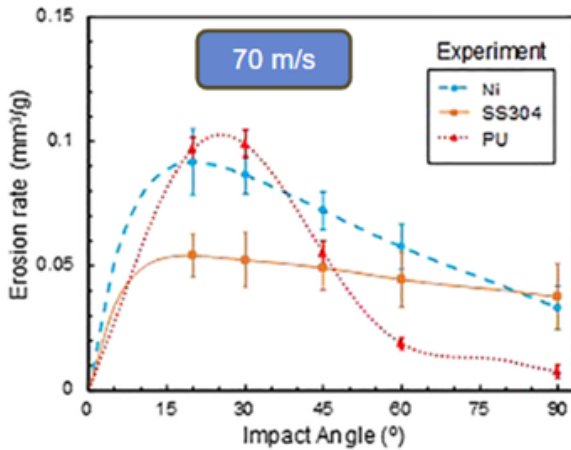


Figure 51: Erosion Rate vs. Impact Angle at an Impact Velocity of 70 m/s [1]

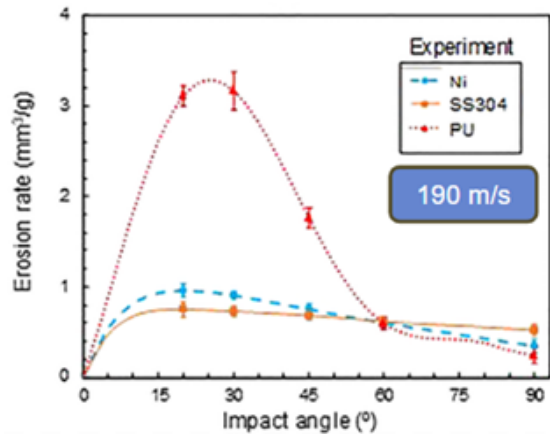


Figure 52: Erosion Rate vs. Impact Angle at an Impact Velocity of 190 m/s [1]

A study conducted by Oka et. al (2005) aimed to investigate erosion impact parameters. The experiment was carried out using a sand-blast-type erosion test rig. The impact angle ranged from 5° to 90°. Three types of particles were used: angular Silica (SiO_2), Silicon Carbide (SiC) and glass beads (GB). The materials tested were an aluminum alloy, copper, iron, carbon steel, and stainless steel. It was found that angular particles (e.g. SiC) cause deeper penetration and more effective material removal compared to round particles (e.g. GB) [16]; this can be seen in Figure 53. Additionally, increased impact velocity or particle diameter will accelerate erosion damage [16].

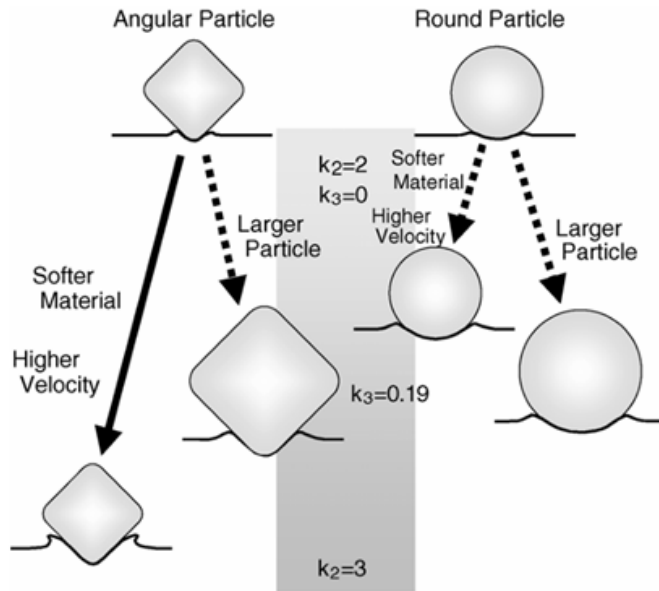


Figure 53: Model of the effects of impact parameters [16]

Helicopter Blade Repairs and Detection Techniques

In a study by Sałaciński et al. (2022), a repair technology for the leading edge of main helicopter rotor blades was developed and validated. The repair technology was tested for use on an Mi-2 helicopter rotor; the structural model of the blade can be seen in Figure 54. The use case for this damage technology is when the protective shield debonds from the leading edge of the blade. An example of a damaged blade can be seen in Figure 55. The repair steps are as follows:

- a) Separation of the damaged piece of shield from the rubber
- b) Sandblasting
- c) Cleaning
- d) Drying
- e) Applying a primer
- f) Applying adhesive paste
- g) Curing
- h) Post-curing

This procedure for leading edge blade repair is depicted in Figure 56. The goal of this repair is to apply a new primer and new epoxy (step e and step f), and use an assembly tool (step g) to clamp down on the leading edge. A schematic of the clamping mechanism can be seen in Figure 57. The group used the Tap Test Method to check the adhesive bond conditions. The goal of this method is to measure sound frequency & amplitude differences between undamaged & damaged bonding plies. A diagram of this test can be seen in Figure 58; the results from the test can be seen in Figure 59. It was found that the repaired bonded joint was 30% weaker than the factory-made joint [20]. According to Sałaciński et al. (2022), the Polish Air Force approved the repair technology for supervised operation in 2019. After two years of operation, there have been no reported issues from the Air Force regarding repaired rotor blades [20].

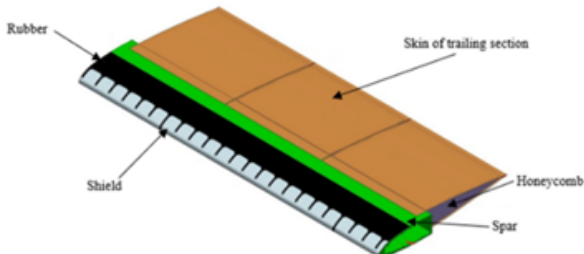


Figure 54: Baseline model of an Mi rotor blade [20]

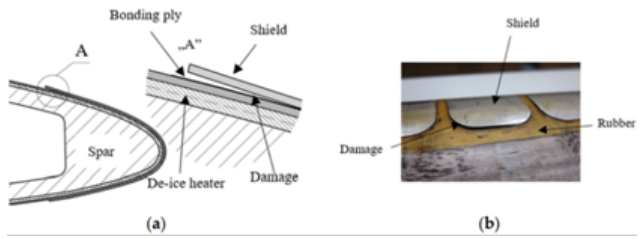


Figure 55: Damage to leading edge- debonding shield. (a) Diagram , (b) Damage to a Mi-2 [20]

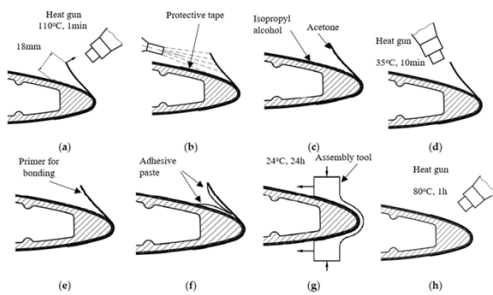


Figure 56: Process of repairing a leading edge [20]

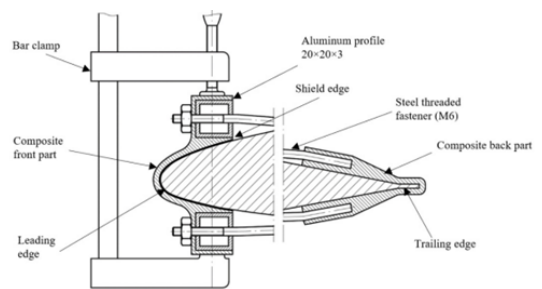


Figure 57: Assembly tool diagram [20]

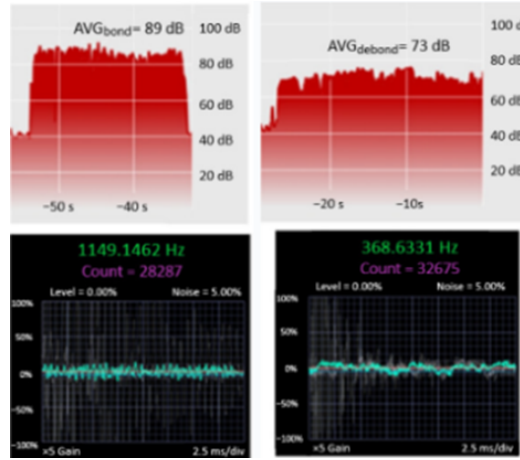
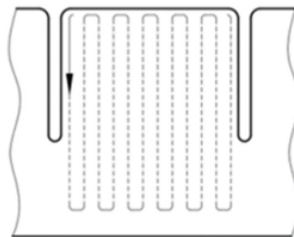
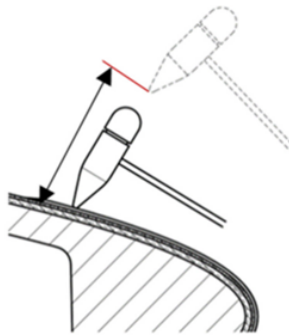


Figure 58: Method of tap-test with inspection hammer [20]

Figure 59: Shield bonded results (left)
Shield disbonded results (right) [20]

In a study conducted by Zheng et al. (2023), Fourier Infrared Analysis (FTIR) was used to detect chemical changes in polyurethane film after erosion. The results in Figure 60 show that the characteristic peaks (e.g., N–H, C=O, and C–O–C) remain largely unchanged. It is stated that no significant chemical changes in the polyurethane film were noticed [5]. This FTIR Method is a valuable technique to infer if a film has reached the end of its service life.

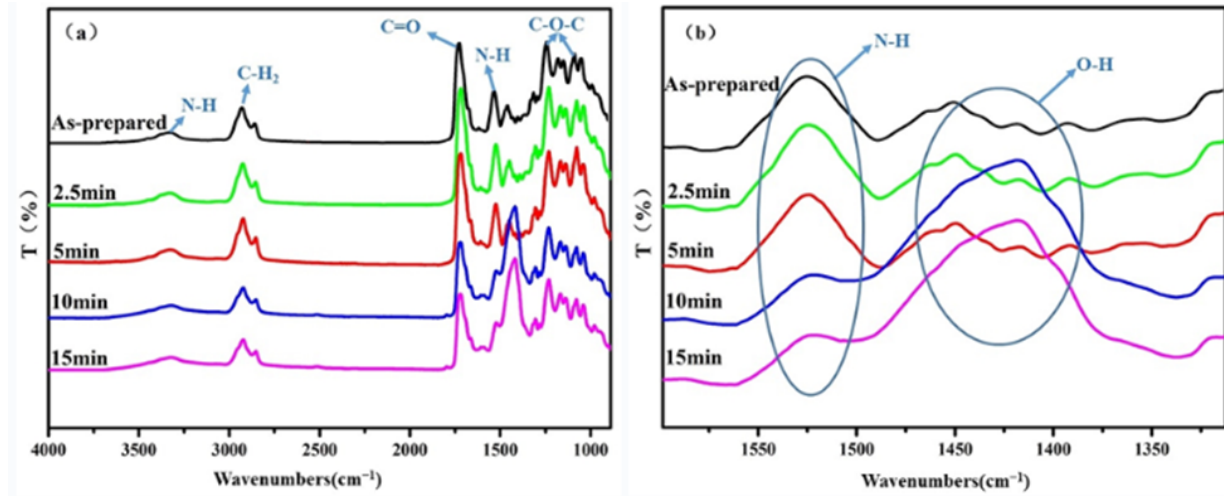


Figure 60: Infrared spectrum of damaged polyurethane after 30° erosion at different times with (a) full infrared image and (b) peak amplification at 1405 cm^{-1} [5]

Conclusion

Research studies on the erosion resistance of helicopter rotor blade materials reveals that erosion resistance is heavily influenced by material composition, particle properties, fiber orientation, and protective coatings or fillers. Fiber-reinforced composites, such as CFRP and GFRP, are valued for their lightweight and high-strength properties. However, their susceptibility to sand erosion depends on several factors, including fiber alignment, resin matrix durability, and filler additives. The multidirectional CFRP configurations mitigate erosion sensitivity compared to unidirectional setups, and silica fume fillers in GFRP enhance resistance by absorbing impact energy. Additionally, it potentially suggests the resin matrix's important role in protecting fibers and improving erosion resistance. Erosion particle size distribution also suggests there's a critical size threshold to be discovered that could significantly affect erosion rate. Most importantly, polyurethane (PU) coatings and elastomers are important solutions for erosion protection on rotor blades. Their ductile behavior, elastic recovery, and self-healing properties from the soft and hard polymer segments allows them to significantly outperform CFRP and GFRP. A key detail is that these elastomers still experience the highest erosion rate (lower resistance) at a specific angle at 30°. While most studies analyzed the effect of various angles on erosion rates, many did not study erosion rates on impact angles under 30°. There is a real possibility where angles lower than 30° could give higher erosion rates. Lastly, the viscoelastic properties of PU strongly correlate with erosion rate, with its loss modulus at high frequencies (~10⁷ Hz) serving as a useful predictive metric. Across these elastomer materials, erosion mechanisms shift from cutting and plowing at low angles to brittle fracture and microcracking at high angles, with impact velocity, erodent size, and exposure time further amplifying damage.

Erosion on metals is influenced by particle size, impact speed, impact angle, and material properties, as demonstrated by both numerical (CFD) and experimental results. It was noted that a higher modulus of elasticity in metal will yield a higher erosion resistance. Additionally, it was observed that erosion mechanisms transitioned from micro-cutting and plowing at low angles to indentation-induced plastic deformation at high angles. The maximum erosion rate for SS304 and Nickel material occurred at 20° (regardless of particle speed). This is an indicator of ductile damage. The face-centered cubic lattice structure of stainless-steel helps make material removal easier. With regards to metallic shielding, the higher erosion resistance of AlTiN is attributed to a combination of higher hardness against micro cutting and higher toughness against crack formation and chipping. Finally, an increased impact velocity or particle diameter will accelerate the erosion damage. During helicopter hover conditions, the blade tips travel 212 – 242 m/s.

Proposal for Future Work

There are still numerous questions left unanswered by these studies. The erosion resistance of polyurethane (PU) elastomers remains understudied and needs further investigation. Key areas that should be explored include PU behavior at a constant high impact velocity and mass flow rate, with a focus on quantifying volume loss and identifying critical erosion particle size thresholds. For instance, to study the critical erosion particle size threshold, all other parameters such as impact velocity, mass flow rate, material properties, particle properties beside particle size should remain constant but at appropriate values. Understanding how particle size influences mass flux and damage mechanisms could bring insights to why erosion rates stabilize beyond a specific threshold. Additionally, erosion rates at low impingement angles under 30° should be systematically studied as well to understand if higher erosion rates beyond 30° exist. This process should also conduct abrasion testing and compare to low angle erosion data. The role of resin matrix materials and fiber to resin ratios in erosion resistance also requires deeper analysis, as these factors could significantly affect fiber-matrix bonding and composite durability. Such studies could explain why some CFRP composites exhibit ductile or brittle damage behavior at different maximum erosion rate impact angles. Importantly, volume loss should be used to assess erosion rates rather than mass loss, as particles may become embedded in the material. At the same time,

additional validation of the loss modulus as a predictive metric for erosion performance is required. Lastly, since elastomers have highest erosion rates at low angles, the shear performance of PU elastomers should be assessed to evaluate their resistance to cutting and plowing actions at low angles.

The aging effects after extreme sand erosion have been mentioned in numerous studies however substantial evidence can still be gathered. Thermal cycling has been a common method for accelerating material aging to understand long-term material degradation and structural integrity. Additionally, environmental conditioning can be carried out by conducting humidity and UV exposure testing. Under intense weather situations, moisture-induced degradation and prolonged sun exposure can damage composite material and rapidly accelerate the erosion of blades. Sand storm simulations can also help provide insight on performance under ultra-high velocity sand impacts. The Kopp-Etchells effect is a phenomenon that causes a ring of light around the rotor blades of helicopters. The ring of light is induced in sandy conditions, when sand strikes the blades and creates sparks. The pyrophoricity of metal shielding on the blades must be examined to ensure this phenomena does not happen; the occurrence of the Kopp-Etchells effect can cause burning of rotor blade coatings, thus affecting the aerodynamics and performance of the helicopter. Furthermore, the effect of blade vibration was not mentioned however it is an important consideration. An increase in blade vibrations could cause more extreme shock impacts of particles, further degrading the blades. Particle rebound has also been discussed however there have been minimal firm conclusions on its impact. An analysis could be done on the damage mechanism of fresh particles versus rebounded particles. Many studies do not specify rotor configurations however this would have a large impact on the degree of particle rebound. For example, single rotor systems may perform differently compared to coaxial rotor systems. A CFD model could be generated to understand the performance of these rotary systems.

Methodology: [ASTM G76-18](#)

Standard Test Method for Conducting Erosion Tests by Solid Particle Impingement Using Gas Jets [21]

- The nozzle tube shall be 1.5 mm +/- 0.075 mm inner diameter and at least 50 mm long.
- The distance from specimen surface to nozzle end shall be 10 +/- 1 mm.
- Nozzle length to diameter ratio should be 25:1 or greater in order to achieve an acceptable particle velocity distribution in the stream
- The test gas shall be nominally dry air. The test report shall indicate the amount of water present in the test gas, at what pressure, and how the measurement was conducted
- System pressure will be approximately 140 kPa, although the pressure will depend on the specific system design
- The test time shall be 10 min to achieve steady state conditions. Longer times are permissible so long as the final erosion crater is no deeper than 1 mm.
- The angle between the nozzle axis and the specimen surface shall be 90 +/- 2°.
- The test temperature shall be the normal ambient value (typically between 18°C to 28°C)
- Particle flux determination requires measurement of the eroded area on the specimen and is subject to considerable error
- Erosion value: Volume loss of specimen material divided by the total mass of abrasive particles that impacted the specimen ($\text{mm}^3 \cdot \text{g}^{-1}$)
- Normalized Erosion Rate: Erosion value ($\text{mm}^3 \cdot \text{g}^{-1}$) of specimen material divided by erosion value ($\text{mm}^3 \cdot \text{g}^{-1}$) of reference material.

References

1. Özen, İ.; Gedikli, H.; Öztürk, B. Improvement of Solid Particle Erosion Resistance of Helicopter Rotor Blade with Hybrid Composite Shield. *Eng. Fail. Anal.* **2021**, *121*, 105175, doi:10.1016/j.engfailanal.2020.105175.
2. Pepi, M.; Squillaciotti, R.; Pfledderer, L.; Phelps, A. Solid Particle Erosion Testing of Helicopter Rotor Blade Materials. *J. Fail. Anal. Prev.* **2012**, *12*, 96–108, doi:10.1007/s11668-011-9531-3.
3. Stachowiak, G.W.; Batchelor, A.W. *Engineering Tribology*; 4th edition.; Elsevier/Butterworth-Heinemann: Oxford, 2014; ISBN 978-0-12-397047-3.
4. Cai, F.; Gao, F.; Pant, S.; Huang, X.; Yang, Q. Solid Particle Erosion Behaviors of Carbon-Fiber Epoxy Composite and Pure Titanium. *J. Mater. Eng. Perform.* **2016**, *25*, 290–296, doi:10.1007/s11665-015-1848-8.
5. Zheng, L.; Fan, J.; Gong, Q.; Sun, W.; Jia, X. Sand Erosion Resistance and Failure Mechanism of Polyurethane Film on Helicopter Rotor Blades. *Polymers* **2023**, *15*, 4386, doi:10.3390/polym15224386.
6. Kang, Y.S.; Park, S.W.; Roh, J.S.; Myong, R.S. Computational Investigation of Effects of Expanded Metal Foils on the Lightning Protection Performance of a Composite Rotor Blade. *Int. J. Aeronaut. Space Sci.* **2021**, *22*, 203–221, doi:10.1007/s42405-020-00288-1.
7. Yao, Y.; Bai, X.; Liu, H.; Li, T.; Liu, J.; Zhou, G. Solid Particle Erosion Area of Rotor Blades: Application on Small-Size Unmanned Helicopters. *Symmetry* **2021**, *13*, 178, doi:10.3390/sym13020178.
8. Leishman, G. *Introduction to Aerospace Flight Vehicles*; Embry-Riddle Aeronautical University, 2023;
9. Kim, A.; Kim, I. Solid Particle Erosion of CFRP Composite with Different Laminate Orientations. *Wear* **2009**, *267*, 1922–1926, doi:10.1016/j.wear.2009.03.038.
10. Öztürk, B.; Gedikli, H.; Kılıçarslan, Y.S. Erosive Wear Characteristics of E-glass Fiber Reinforced Silica Fume and Zinc Oxide-filled Epoxy Resin Composites. *Polym. Compos.* **2020**, *41*, 326–337, doi:10.1002/polc.25372.
11. Cizmas, P.G.; Slattery, J.C. Dimensionless Correlation for Sand Erosion of Families of Polymers. *Wear* **2007**, *262*, 316–319, doi:10.1016/j.wear.2006.05.008.
12. Arena, G.; Friedrich, K.; Acierno, D.; Padenko, E.; Russo, P.; Filippone, G.; Wagner, J. Solid Particle Erosion and Viscoelastic Properties of Thermoplastic Polyurethanes. *Express Polym. Lett.* **2015**, *9*, 166–176, doi:10.3144/expresspolymlett.2015.18.
13. Guo, X.; Zang, F.; Zhu, Y.; Cao, D. Aircraft Propeller Erosion Wear and Aerodynamic Characteristics. *Acta Mech. Sin.* **2025**, *41*, 524251, doi:10.1007/s10409-024-24251-x.
14. Bai, X.; Yao, Y.; Han, Z.; Zhang, J.; Zhang, S. Study of Solid Particle Erosion on Helicopter Rotor Blades Surfaces. *Appl. Sci.* **2020**, *10*, 977, doi:10.3390/app10030977.
15. Yang, Z.; Chen, J.; He, G.; Liang, X.; Luo, S. Mechanical Properties and Sand Erosion Damage Mechanism of TiN/Ti Multilayer Coatings after Thermal Cycling Treatment. *J. Mater. Eng. Perform.* **2023**, *32*, 8775–8785, doi:10.1007/s11665-022-07759-4.
16. Oka, Y.I.; Okamura, K.; Yoshida, T. Practical Estimation of Erosion Damage Caused by Solid Particle Impact. *Wear* **2005**, *259*, 95–101, doi:10.1016/j.wear.2005.01.039.

17. Nguyen, Q.B.; Nguyen, V.B.; Lim, C.Y.H.; Trinh, Q.T.; Sankaranarayanan, S.; Zhang, Y.W.; Gupta, M. Effect of Impact Angle and Testing Time on Erosion of Stainless Steel at Higher Velocities. *Wear* **2014**, *321*, 87–93, doi:10.1016/j.wear.2014.10.010.
18. Özen, İ.; Gedikli, H. Solid Particle Erosion on Shield Surface of a Helicopter Rotor Blade Using Computational Fluid Dynamics. *J. Aerosp. Eng.* **2019**, *32*, 04018131, doi:10.1061/(ASCE)AS.1943-5525.0000962.
19. Yang, Q.; Pankov, V. Solid Particle Erosion Performance and Damage Mechanism of AlTiN Coating. *Tribol. Trans.* **2023**, *66*, 809–821, doi:10.1080/10402004.2023.2224839.
20. Sałaciński, M.; Puchała, K.; Leski, A.; Szymczyk, E.; Hutsaylyuk, V.; Bednarz, A.; Synaszko, P.; Kozera, R.; Olkowicz, K.; Głowacki, D. Technological Aspects of a Reparation of the Leading Edge of Helicopter Main Rotor Blades in Field Conditions. *Appl. Sci.* **2022**, *12*, 4249, doi:10.3390/app12094249.
21. ASTM International ASTM G76-18 Standard Test Method 2018.